Applied Materials Today 35 (2023) 101953

Contents lists available at ScienceDirect

Applied Materials Today

journal homepage: www.elsevier.com/locate/apmt

Controlling molecular self-assembly of inverse-phosphocholine lipids at oxide interfaces with divalent cations

Tun Naw Sut [a,b], Soohyun Park [a], Joshua A. Jackman [b,*], Nam-Joon Cho [a,*]

[a] School of Materials Science and Engineering, Nanyang Technological University, 50 Nanyang Avenue, Singapore 639798, Singapore
[b] School of Chemical Engineering and Translational Nanobioscience Research Center, Sungkyunkwan University, Suwon 16419, Republic of Korea

ARTICLE INFO

Keywords:
Inverse-phosphocholine lipid
Divalent cation
Vesicle fusion
Quartz crystal microbalance-dissipation
Fluorescence recovery after photobleaching

ABSTRACT

Sub-100 nm vesicles composed of inverse-phosphocholine (CP) lipids are versatile building blocks for interfacing with inorganic material surfaces and demonstrate unique chemical functionalities due to outward-facing phosphate groups. Compared to typical phospholipids, the surface presentation of CP lipids has enabled new covalent possibilities like click chemistry for drug delivery and imaging applications while utilizing this phosphate chemistry in noncovalent self-assembly contexts remains unexplored. Herein, we report that the presence of phosphate-binding divalent cations such as Ca^{2+} and Mg^{2+} can dramatically shift the self-assembly behavior of CP lipid vesicles on TiO_2 and SiO_2 surfaces, inhibiting spontaneous supported lipid bilayer (SLB) formation on TiO_2 in cases where it typically occurs and promoting SLB formation on SiO_2 in cases where lipid adsorption is otherwise negligible. Quartz crystal microbalance-dissipation (QCM-D) measurements were performed to track the corresponding adsorption kinetics and self-assembly outcomes. Importantly, an optimal combination of CP lipid fraction in vesicles and specific divalent cation type was also identified, which enabled SLB formation on both TiO_2 and SiO_2 surfaces under equivalent conditions. SLB fluidity on SiO_2 surfaces was additionally confirmed by fluorescence recovery after photobleaching (FRAP) experiments. We rationalize these molecular-level phenomena in terms of vesicle stability and lipid-surface interactions, demonstrating a versatile approach to control CP lipid self-assembly with divalent cations.

1. Introduction

Inverse-phosphocholine (CP) lipids are a relatively new, emerging class of synthetic phospholipid with broad utility across biotechnology and materials science applications [1–10]. Compared to zwitterionic phosphocholine (PC) lipids that are a major component of cellular membranes, the headgroup of CP lipids has the phosphate and choline groups reversed whereby the phosphate group is presented outwards and imparts CP lipids with anionic character. Perttu *et al.* first described the synthesis of CP lipids and reported that CP lipids maintained a negative surface potential across a wide pH range and aggregated in the presence of Ca^{2+} ions [1]. The charge flipping in CP lipids has enabled new possibilities for controlling covalent interactions with nanomaterials [2,3,6] and for drug delivery applications [4,5,7,9]. From a material science perspective, one promising application is the fabrication of CP-based supported lipid bilayers (SLBs) that are durable coatings and can enable antifouling properties along with orthogonal chemistry possibilities for surface functionalization [11,12].

In the course of studying SLB coating formation on oxide nanoparticles, it was discovered that 2-((2,3-bis(oleoyloxy)propyl)dimethylammonio)ethyl hydrogen phosphate (DOCP) lipid vesicles readily form SLBs on TiO_2 nanoparticles by fusion whereas there is no vesicle fusion with SiO_2 nanoparticles owing to strong charge repulsion [3]. In addition, it was shown that SLBs formed on TiO_2 nanoparticles are more stable than those formed by noncovalently attached, zwitterionic 1,2-dioleoyl-*sn*-glycero-3-phosphocholine (DOPC) lipids on SiO_2 nanoparticles. To rationalize these distinct stabilities, it has been discussed how the phosphoryl oxygen atom of the exposed phosphate group is responsible for covalent binding of DOCP lipids to metal oxide surfaces [13]. More specifically, DOCP lipids directly bind to TiO_2 *via* P-O-Ti bond formation whereas steric hindrance caused by the choline group of PC lipids inhibits direct phosphate group binding to SiO_2. DOCP SLBs can also be formed on other types of oxide nanoparticles such as Fe_3O_4, ZrO_2, Y_2O_3, ITO, In_2O_3 and Mn_2O_3 [2]. Recently, we demonstrated that DOCP lipid vesicles can also form SLBs on flat, macroscopic TiO_2 surfaces in pH 7.5 conditions and described a two-step mechanism in which

* Corresponding authors.
E-mail addresses: jjackman@skku.edu (J.A. Jackman), njcho@ntu.edu.sg (N.-J. Cho).

https://doi.org/10.1016/j.apmt.2023.101953
Received 11 August 2023; Received in revised form 28 September 2023; Accepted 2 October 2023
Available online 13 October 2023

noncovalent interfacial forces mediate initial adsorption followed by covalent bonding that drives vesicle fusion and subsequent lipid re-assembly [14]. Notably, DOCP lipid vesicles did not adsorb onto SiO_2 surfaces in the same conditions and thus it was not possible to form DOCP SLBs on SiO_2. More recent work has revealed that noncovalently attached DOCP SLBs can be formed on SiO_2 surfaces in a specific set of low pH and high salt conditions while DOCP lipid vesicle adsorption can be repelled on TiO_2 surfaces in high pH conditions, demonstrating that modulation of different vesicle-surface interaction types is an important determinant of CP lipid self-assembly outcomes [15].

These findings motivate deeper investigation of how DOCP lipid self-assembly can be modulated on oxide surfaces, especially considering that the exposed phosphate group possesses noncovalent functionalization possibilities such as divalent cation binding. Indeed, in various lipid systems, the type and concentration of ions in the bulk solution has been shown to control vesicle adsorption and SLB formation processes [16–19]. Pioneering work on negatively charged 1,2-dioleoyl-*sn*-glycero-3-phospho-L-serine (DOPS) lipid vesicles demonstrated that divalent cations can promote SLB formation on TiO_2 by forming ionic bridges between the carboxylic acid headgroups of lipid molecules and hydroxyl groups on the surface [18]. It has also been demonstrated that divalent cations can increase vesicle-surface interactions and cause greater deformation of adsorbed DOPC lipid vesicles on TiO_2 and SiO_2 surface [20]. In addition to affecting vesicle-surface interactions, divalent cations can influence vesicle-vesicle interactions [16,20]. Anionic lipid vesicles tend to aggregate and/or fuse in the presence of divalent cations because the outer leaflet of vesicles are joined together by ion bridging [21,22]. In the context of CP lipids, it has been reported that metal ions such as calcium [1], cadmium [23], zinc [24] and copper [25] can trigger DOCP lipid vesicle aggregation, however, the extent to which divalent cations can control DOCP lipid self-assembly on oxide surfaces remains unexplored.

In this study, our objective was to investigate how divalent cations affect DOCP lipid vesicle interactions with TiO_2 and SiO_2 surfaces in order to rationally control lipid self-assembly processes on the two surfaces. Quartz crystal microbalance-dissipation (QCM-D) measurements were conducted to track lipid vesicle adsorption kinetics while fluorescence recovery after photobleaching (FRAP) experiments were employed to characterize lipid attachment in select cases. We tested two types of divalent cations (Ca^{2+} and Mg^{2+}) and three different DOCP lipid fractions in order to identify conditions in which lipid adsorption was inhibited along with conditions where SLB formation was simultaneously possible on both surfaces. In some cases, the self-assembly behavior depended on the ion type while other cases were more generalizable. While covalent and noncovalent chemistries have been previously identified as key factors in driving DOCP lipid vesicle adsorption and rupture to form SLBs, our findings demonstrate how a third type of chemical interaction, i.e., ionic bridging interactions mediated by divalent cations, can play a critical and deterministic role in modulating self-assembly behavior on oxide surfaces.

2. Materials and methods

2.1. Reagents

DOCP, DOPC and 1,2-dioleoyl-*sn*-glycero-3-phosphoethanolamine-N-(lissamine rhodamine B sulfonyl) (ammonium salt) (Liss Rhod PE) lipids dissolved in chloroform were obtained from Avanti Polar Lipids, Inc. (Alabaster, AL). The molecular structures of DOCP and DOPC lipids are presented in Fig. 1. Ethylenediaminetetraacetic acid (EDTA) and other reagents were purchased from Sigma-Aldrich (St Louis, MO). Milli-Q-treated water (>18 MΩ·cm) (MilliporeSigma, Billerica, MA) was used to prepare all buffer solutions.

2.2. Vesicle preparation

Vesicles were prepared by the extrusion method, as previously described [26]. Lipids mixed to the desired molar ratio in a glass vial were dried with nitrogen gas to form a dried lipid film, and then stored in a vacuum desiccator overnight to remove residual chloroform. Afterwards, the dried lipid film was hydrated in aqueous buffer (10 mM Tris, 150 mM NaCl, pH 7.5) to a 5 mg/mL stock concentration and vortexed for 3 min to form multilamellar vesicles. Then, a Mini-Extruder (Avanti Polar Lipids) was used to extrude vesicles by passing them through a polycarbonate membrane with 50 nm-diameter pores for a total of 31 times, which yielded unilamellar vesicles. Before each experiment, the stock vesicles were diluted in the appropriate buffer to 0.1 mg/mL.

2.3. Quartz crystal microbalance-dissipation (QCM-D)

Vesicle adsorption kinetics were monitored with a Q-Sense E4 instrument (Biolin Scientific AB, Gothenburg, Sweden). Before each measurement, the sensor chip surfaces were rinsed with water and ethanol, dried with nitrogen gas, and treated with oxygen plasma for 1 min (SiO_2) or 3 min (TiO_2) in an Expanded Plasma Cleaner (PDC-002, Harrick Plasma, Ithaca, NY). Sample solutions were added continuously into the measurement chamber using a peristaltic pump (Reglo Digital MS-4/6, Ismatec, Glattbrugg, Switzerland) at a nominal rate of 50 μL/min. Each measurement chamber was maintained at the temperature of

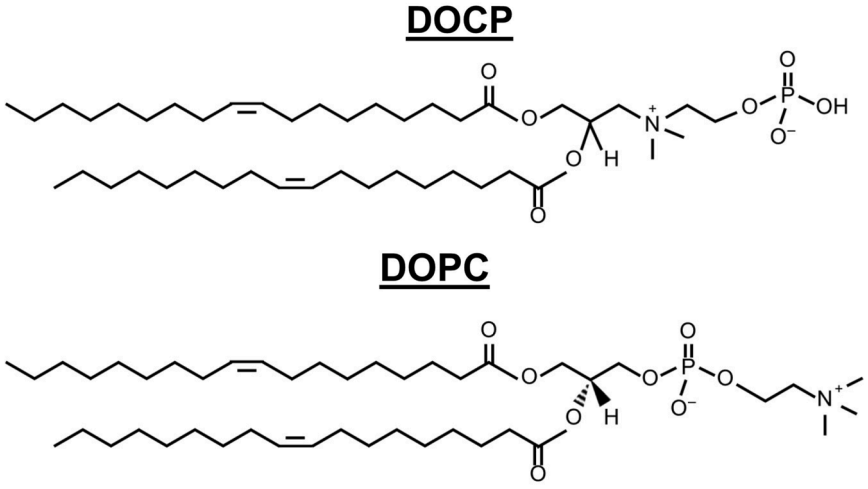

Fig. 1. Molecular structures of DOCP and DOPC lipids. Note the difference in headgroup chemistry while the chains are equivalent.

25.0 ± 0.5 °C. The shifts in resonance frequency (Δf) and energy dissipation (ΔD) of the sensor chips were recorded as a function of time at odd overtones. The presented data are from the 5th overtone and were normalized according to the overtone number. Data processing was completed using the Q-Tools (Biolin Scientific AB) and OriginPro (OriginLab, Northampton, MA) software programs.

2.4. Dynamic light scattering (DLS)

The DLS technique was employed to measure the size distribution of suspended lipid vesicles, as previously described [27]. A 90Plus particle size analyzer instrument (Brookhaven Instruments Corporation, Holtsville, NY) with a 658.0 nm monochromatic laser was used and the scattered light at 90° was measured. The mean hydrodynamic diameter and standard deviation of the vesicles were obtained from five measurements. For each DLS experiment, the stock vesicles were diluted to 0.1 mg/mL and vesicle stability was assessed by measuring vesicle size as a function of incubation time in the appropriate buffer solution. The time at which the vesicles were diluted is indicated as $t = 0$ min.

2.5. Fluorescence recovery after photobleaching (FRAP)

Lateral lipid diffusivity in SLBs was measured using the fluorescence recovery after photobleaching (FRAP) technique, as previously described [28]. For FRAP experiments, 0.5 mol% fluorescent lipid (Liss Rhod PE) was included in the precursor lipid vesicles and experiments were conducted in a flow-through microfluidic chamber. Liquid sample introduction was fixed at a flow rate of 50 μL/min by a peristaltic pump (Reglo Digital MS-4/6). Upon SLB formation, a 20 μm diameter circular spot in the SLB was photobleached for 5 s with a 532 nm, 100 mW laser (Coherent Inc., Santa Clara, CA). Time-lapse image snapshots were then collected from minus 1 s (before bleaching) to 120 s at 2 s intervals to monitor recovery of the fluorescence signal. The diffusion coefficient of lateral lipid mobility was calculated by the Hankel transform method [29]. The mean and standard deviation of diffusion coefficient values were obtained from at least five different SLB regions per condition. All measurements were conducted at room temperature (~25 °C).

3. Results and discussion

3.1. Experimental design

Experiments were performed in 10 mM Tris buffer (pH 7.5) containing 150 mM NaCl without or with 5 mM $MgCl_2$ or $CaCl_2$. The tested lipid compositions were inspired by our past study [14] and chosen to include cases where SLB formation, intact vesicle adlayer formation, or no adsorption occurred in divalent cation-free conditions. In particular, we previously demonstrated that, for vesicles composed of a mixture of DOCP and DOPC lipids, an intact vesicle adlayer was formed on TiO_2 for vesicles containing 25 mol% DOCP, while SLB formation occurred on TiO_2 for vesicles containing ≥ 50 mol% DOCP. On the other hand, SLB formation occurred on SiO_2 for vesicles containing ≤ 25 mol% DOCP whereas no adsorption occurred on SiO_2 for vesicles containing ≥ 50 mol% DOCP. Thus, we selected 100 mol% DOCP lipid vesicles along with 25/75 mol% DOCP/DOPC and 12.5/87.5 mol% DOCP/DOPC as three representative compositions to test the effects of divalent cations on modulating vesicle adsorption behavior.

3.2. Vesicle stability measurements

We initially characterized the effects of divalent cations on DOCP lipid vesicle properties in solution by dynamic light scattering (DLS) measurements. As mentioned above, it has been previously observed that Ca^{2+}ions induce aggregation of 100 mol% DOCP lipid vesicles by forming ion bridges between DOCP lipid headgroups [1]. To expand on this observation, we investigated the size stability of the three tested vesicle compositions in the presence of Mg^{2+} or Ca^{2+} ions. Control experiments and the initial preparation of the stock vesicle samples were performed in equivalent buffer solution without divalent cations. Before each measurement series, an aliquot of the stock vesicle sample was diluted in the appropriate buffer. Upon dilution, DLS measurements were conducted periodically over a 120-min timespan.

Fig. 2**A** presents the results of DLS measurements using 100 mol% DOCP lipid vesicles in different buffer conditions. No vesicle aggregation was observed in the control case, as indicated by a consistent vesicle diameter of ~70 nm across the entire timespan. In the Mg^{2+}case, the vesicle size increased immediately after dilution ($t = 0$ min) from ~70 nm to ~1200 nm, indicating vesicle fusion/aggregation due to the presence of Mg^{2+}ions. A continual increase in vesicle size was observed and, after 120 min of incubation, the mean diameter was around ~2000 nm. In the Ca^{2+}case, a similar trend of increasing vesicle size and aggregation was observed, changing from ~70 nm to ~1260 nm immediately upon dilution and reaching ~2175 nm by the end of the 120-min incubation period. Thus, both types of divalent cations rapidly promoted aggregation of 100 mol% DOCP lipid vesicles in solution.

By contrast, $Mg^{2+}$and Ca^{2+} did not cause appreciable vesicle fusion/aggregation of 25/75 mol% DOCP/DOPC lipid vesicles (Fig. 2**B**). The size of the vesicles remained stable at ~70 nm over the whole incubation period in the control case, indicating no aggregation. Immediately after dilution in Mg^{2+}-containing buffer, the vesicle size increased slightly from ~70 nm to ~83 nm, and remained consistent at ~108 nm from 30 min onwards. In the Ca^{2+}case, the initial size increase was comparable to that in the Mg^{2+}case and a stable size around ~92 nm was achieved after 15 min. Since the vesicles had 75 mol% zwitterionic DOPC lipids, the negative surface charge of the lipid vesicles along with the exposed phosphate group density was insufficient for the divalent cations to induce bridging-related vesicle aggregation.

In addition, for 12.5/87.5 mol% DOCP/DOPC lipid vesicles, the measurement results showed no size increase in all cases (Fig. 2**C**). The average vesicle size was ~70 nm over the entire incubation period, indicating that the bridging effect of the divalent cations is negligible at 12.5 mol% DOCP. Altogether, the DLS results support that the bridging effect of divalent cations on DOCP lipid vesicles in solution is reduced with decreasing DOCP molar fraction: while 100 mol% DOCP lipid vesicles aggregated in bulk solution, the 25/75 mol% DOCP/DOPC lipid vesicles experienced only minor size changes and 12.5/87.5 mol% DOCP/DOPC lipid vesicles negligible size changes.

In addition to bridging-related vesicle aggregation effects, it is noteworthy that divalent cations can influence the mechanical properties of solution-phase, individual lipid vesicles. Indeed, it has been reported that divalent cations tend to increase membrane rigidity and phase transition temperature while also inducing membrane phase separation in some cases [30–32]. For negatively charged lipid vesicles, electrostatic interactions are mainly responsible for the binding of divalent cations to anionic lipid headgroups, which can contribute to an increase in membrane rigidity [33,34]. By contrast, for zwitterionic lipid vesicles, divalent cations enhance membrane rigidity at high concentrations exceeding 1 M but typically exhibit negligible effects at lower concentrations [35,36]. In the context of our experimental conditions, we can infer from these previously reported trends that individual 100 mol% DOCP lipid vesicles would possibly be more rigid in the presence of divalent cations compared to 25/75 mol% DOCP/DOPC lipid vesicles and 12.5/87.5 mol% DOCP/DOPC lipid vesicles but bridging-related aggregation appears to be the dominant factor driving fusogenicity in line with the DLS results.

3.3. Vesicle adsorption kinetics

We next studied the effects of divalent cations on DOCP lipid vesicle adsorption onto TiO_2 and SiO_2 surfaces by performing QCM-D experiments. The QCM-D technique tracks the kinetics of vesicle adsorption by measuring changes in resonance frequency (Δf) and energy dissipation

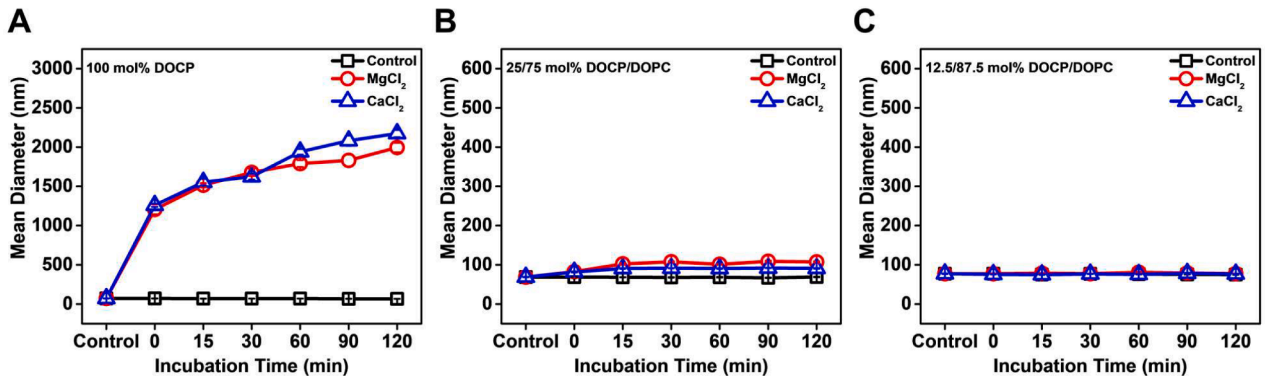

Fig. 2. DLS measurements of vesicle stability in presence of divalent cations. The mean diameter of vesicles was measured as a function of incubation time for **(A)** 100 mol% DOCP vesicles, **(B)** 25/75 mol% DOCP/DOPC vesicles, and **(C)** 12.5/87.5 mol% DOCP/DOPC vesicles. Stock vesicles prepared and diluted in buffer without divalent cations were used for the control measurements (black lines with squares). The stock vesicles were then diluted in the appropriate buffer and the vesicle size was measured periodically over the incubation period of 120 min. $t = 0$ min indicates the time point when vesicles were diluted. The mean ± standard deviation are reported from five technical replicates.

(ΔD) as a function of time. The mass of the adsorbed lipid layer is related to the Δf shift and its viscoelastic properties are reflected in the ΔD shift (relative to a buffer baseline, $\Delta f = \sim -25$ Hz and $\Delta D < 1 \times 10^{-6}$ are typical for a complete SLB) [37]. In all experiments, a baseline signal was first established in the appropriate buffer without vesicles. The buffer used in the control experiments had no divalent cations. Next, 0.1 mg/mL vesicles in an identical buffer were added at $t = 5$ min until reaching stable responses. Then, a buffer washing step was performed for 10 min to remove weakly adsorbed lipids. The final Δf and ΔD after buffer washing are reported below.

3.3.1. *Vesicles containing 100 mol% DOCP lipid*

Figs. 3**A** and 3**B** show the adsorption kinetics of 100 mol% DOCP vesicles on TiO_2 and SiO_2 surfaces, respectively. The final Δf and ΔD shifts are also summarized in Figs. 3**C** and 3**D**, respectively. On TiO_2, SLB formation occurred in the control case (no divalent cations) and the corresponding Δf and ΔD shifts were around −25 Hz and 0.2×10^{-6}, respectively. In the Mg^{2+} case, nearly negligible vesicle adsorption

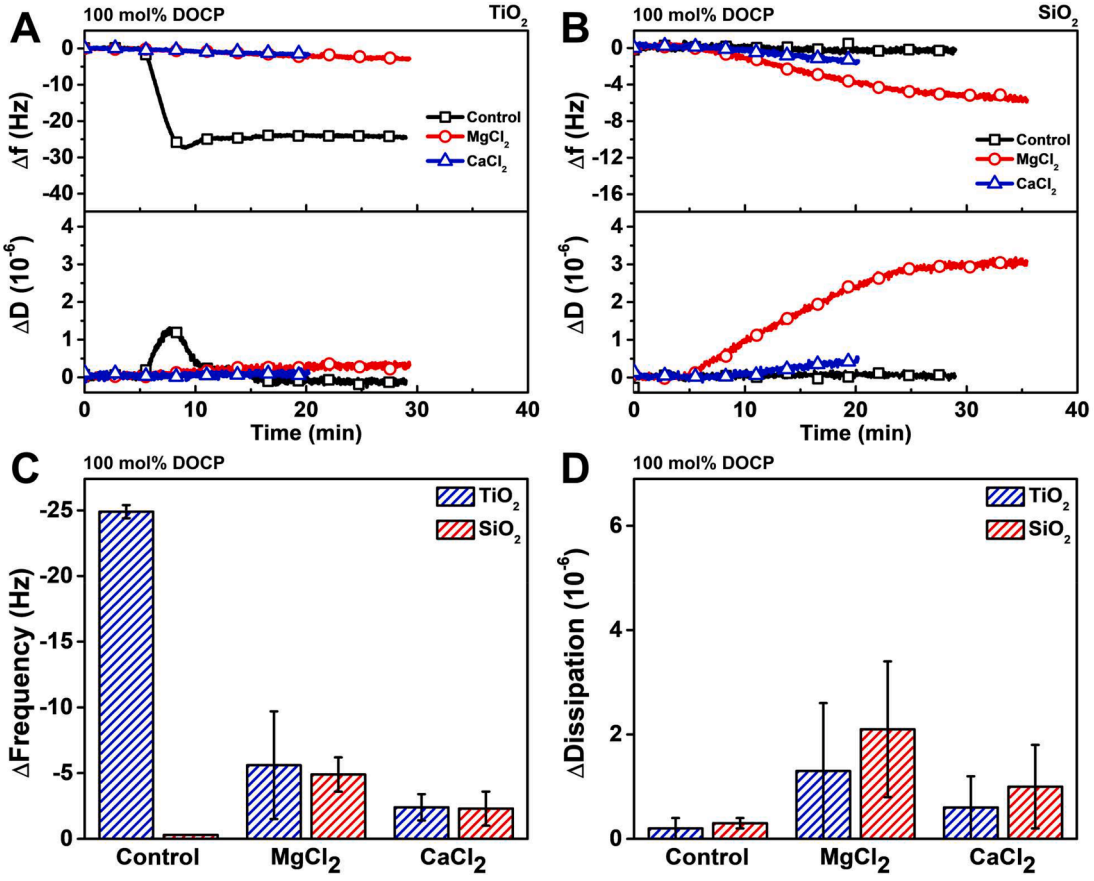

Fig. 3. QCM-D measurements tracking 100 mol% DOCP lipid vesicle adsorption onto TiO_2 and SiO_2 surfaces and divalent cation effects. Frequency (Δf) and energy dissipation (ΔD) shifts were tracked as a function of time on **(A)** TiO_2 and **(B)** SiO_2 surfaces. The baseline was established in appropriate buffer and vesicles were added at $t = 5$ min. The control experiment was conducted in buffer without divalent cations. Summary of final **(C)** Δf and **(D)** ΔD shift values for vesicle adsorption in different buffer conditions. The mean ± standard deviation are reported from three independent measurements.

occurred and the final Δf and ΔD shifts were about −6 Hz and 0.2 × 10^{-6}, respectively. There was even lower vesicle adsorption in the presence of Ca^{2+} and the resulting Δf and ΔD shifts were around −2 Hz and 0.5 × 10^{-6}, respectively. In the presence of both divalent cation types, vesicle-vesicle interactions in the bulk solution are heightened as shown above, leading to greater aggregation that likely impeded the interaction of individual vesicles with the oxide surfaces and thus negated SLB formation through typical adsorption pathways.

Likewise, on SiO_2, 100 mol% DOCP lipid vesicles did not adsorb in the absence of divalent cations, as indicated by Δf and ΔD shifts around −0.3 Hz and 0.3 × 10^{-6}, respectively, for the control case. This result is expected since the interaction between DOCP lipid vesicles and SiO_2 is repulsive [3,14]. In the presence of Mg^{2+}, vesicles adsorbed weakly, with final Δf and ΔD shifts around −5 Hz and 2.1 × 10^{-6}, respectively. As in the TiO_2 case, even weaker adsorption occurred in the presence of Ca^{2+} and the final Δf and ΔD shifts were around −2 Hz and 1.0 × 10^{-6}, respectively. Interestingly, compared to the control case on SiO_2, divalent cations slightly aided DOCP lipid attachment to the SiO_2 surface but the effect was still minor.

Across both surfaces, it is also interesting that Mg^{2+} ions tended to cause larger Δf and ΔD shifts than Ca^{2+} ions. The effect was most evident in the ΔD shift response, suggesting that the attached lipid molecules were in a loosely packed configuration since rigid adlayers such as a complete SLB typically result in ΔD shifts below 1 × 10^{-6} [37]. Nevertheless, divalent cations impeded 100 mol% DOCP lipid vesicle adsorption on both surfaces, supporting that it is preferable to form DOCP SLBs on TiO_2 in the absence of divalent cations and suggesting that other ways be developed to improve DOCP lipid attachment on SiO_2.

To rationalize the lack of vesicle adsorption observed in the presence of divalent cations, there are two possible contributing factors in terms of vesicle-surface interactions and bulk vesicle diffusion. First, it should be emphasized that the adsorption of negatively charged lipid vesicles must overcome electrostatic and steric-hydration repulsive forces with oxide surfaces, even in cases where the primary binding mode of eventual lipid attachment is covalent [14]. In the case of 100 mol% DOCP lipid vesicles, divalent cations directly bind to the exposed phosphate headgroups, which causes vesicle aggregation and potentially charge neutralization or even conferral of positive charge to the lipid-cation fused aggregates. On the other hand, divalent cations also bind to the oxide surface [38] and render it more positively charged, which could potentially lead to electrostatic repulsion between the lipid-cation aggregates and oxide surface. In addition, the significant increase in the size of vesicle aggregates caused by divalent cations and corresponding decrease in the number of diffusing species may hinder appreciable lipid attachment to the surface within the experimental time scale.

3.3.2. *Vesicles containing 25 mol% DOCP lipid*

Fig. 4 presents the adsorption kinetics of 25/75 mol% DOCP/DOPC lipid vesicles on TiO_2 and SiO_2 surfaces along with summarized final Δf and ΔD shift values. Vesicles adsorbed onto TiO_2, leading to final Δf and ΔD values around −63 Hz and 7 × 10^{-6}, respectively, in the control case (Fig. 4**A**). A slight inflection point in the adsorption kinetics indicates incomplete rupture of adsorbed vesicles and occurs due to release of hydrodynamically coupled solvent from vesicle interiors upon rupture [39]. In the Mg^{2+} case, vesicle adsorption also occurred and caused final Δf and ΔD shifts around −41 Hz and 3 × 10^{-6}, respectively. The inflection point was more pronounced, indicating more extensive vesicle rupture upon reaching a critical coverage of adsorbed vesicles on the

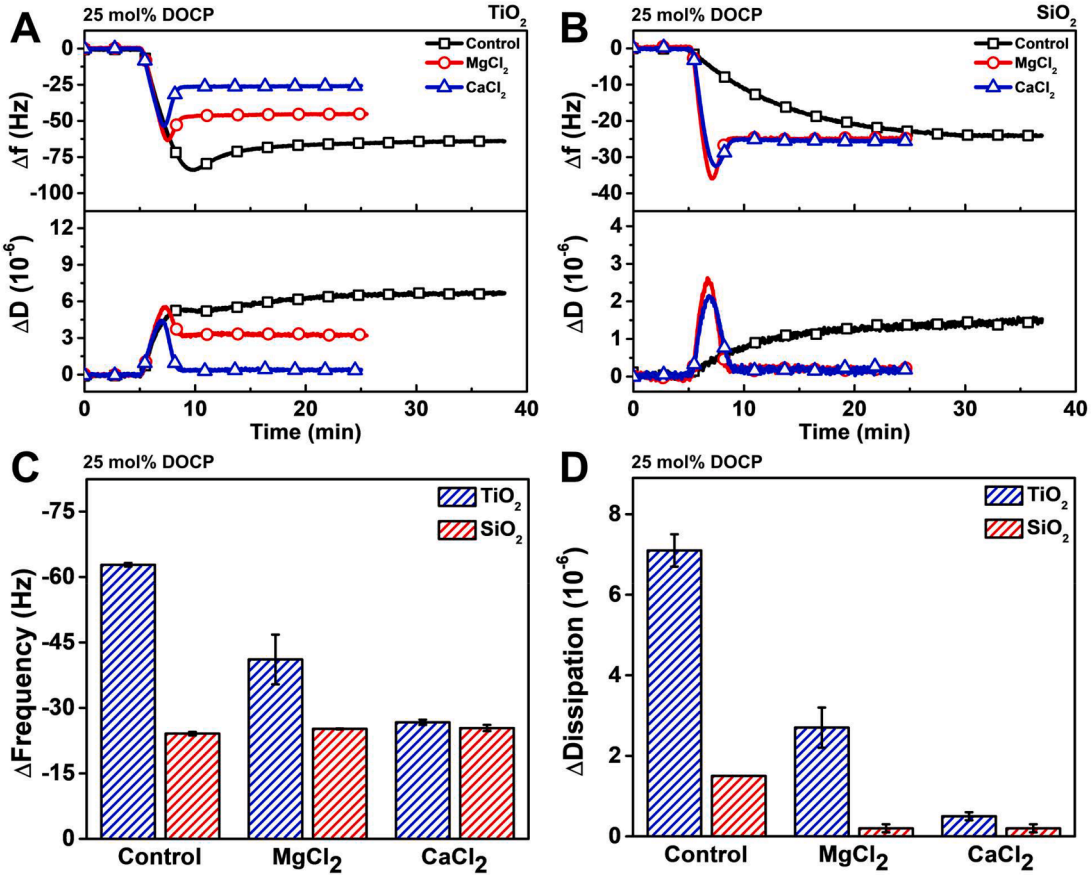

Fig. 4. QCM-D measurements tracking 25 mol% DOCP lipid vesicle adsorption onto TiO_2 and SiO_2 surfaces and divalent cation effects. The lipid composition of the vesicles was 25/75 mol% DOCP/DOPC and the panels are depicted as in Fig. 3.

surface. Interestingly, in the Ca^{2+} case, an SLB was formed with a clearly demarcated inflection point indicative of two-step kinetics, *i.e.*, vesicles adsorbed until reaching a critical surface coverage followed by spontaneous rupture. The final Δf and ΔD values were around −26 Hz and 0.5 × 10^{-6}, respectively, which indicate SLB formation [37]. Together, these results indicate a transition in adsorption pathway across the three cases from weak vesicle rupture in the control case to more appreciable vesicle rupture in the Mg^{2+} case to complete vesicle rupture and SLB formation in the Ca^{2+} case.

Of note, a lower critical surface coverage of adsorbed vesicles was needed to trigger 25 mol% DOCP lipid vesicle rupture on TiO_2 in the presence of Ca^{2+} ions since the inflection point occurred at Δf ∼ −54 Hz and ΔD ∼ 4 × 10^{-6} for that case. By contrast, the inflection point occurred at Δf ∼ −64 Hz and ΔD ∼ 5 × 10^{-6} in the presence of Mg^{2+} ions, which indicate a higher necessary surface coverage. This finding is consistent with past reports discussing how Ca^{2+} ions improve vesicle-surface interactions to a greater extent than Mg^{2+} ions for zwitterionic DOPC lipid vesicles on TiO_2 and SiO_2 surfaces [20].

On SiO_2, one-step adsorption kinetics with final Δf and ΔD shift values around −24 Hz and 1.5 × 10^{-6}, respectively, were observed in the control case (Fig. 4**B**). The large ΔD shift indicated lipid adsorption occurred, albeit without complete SLB formation. That is, the corresponding QCM-D adsorption kinetics indicate that at least some adsorbed lipid vesicles remain unruptured as complete SLB formation typically results in final ΔD shifts less than 1 × 10^{-6} [37]. In marked contrast, there was a clear transition to two-step adsorption kinetics in the presence of divalent cations. In those cases, vesicles adsorbed onto the surface until reaching a critical surface coverage, as denoted by inflection points in the QCM-D signals. The Δf and ΔD shift values at the critical coverage in the Mg^{2+} case were around −36 Hz and 2.5 × 10^{-6}, respectively, and in the Ca^{2+} case were around −33 Hz and 2 × 10^{-6}, respectively. The smaller critical coverage values in the Ca^{2+} case points to a greater extent of vesicle deformation due to stronger vesicle-surface interactions [40]. In both divalent cation cases, the final Δf and ΔD shift values indicated SLB formation (Δf ∼ −25 Hz and ΔD ∼ 0.2 × 10^{-6}).

These results show that divalent cations increased the vesicle-surface interaction strength on both surfaces and led to successful SLB formation on TiO_2 with Ca^{2+} and on SiO_2 with both Mg^{2+} and Ca^{2+} (Figs. 4**C,D**). The distinct effects of Mg^{2+} and Ca^{2+} ions in promoting SLB formation in a surface-selective manner support that lipid-ion-surface bridging interactions play an important role in driving vesicle-surface interactions in an ion type-specific manner. Furthermore, compared to 100 mol% DOCP lipid vesicles, 25 mol% DOCP lipid vesicles are stable in the presence of divalent cations according to the DLS data, which indicates that aggregation mediated by vesicle-vesicle interactions in the bulk solution are negligible in this system.

3.3.3. *Vesicles containing 12.5 mol% DOCP lipid*

Fig. 5 presents the adsorption kinetics of 12.5/87.5 mol% DOCP/DOPC lipid vesicles on TiO_2 and SiO_2 surfaces along with summarized final Δf and ΔD shift values. On TiO_2, one-step adsorption kinetics with a monotonic decrease in the Δf signal and corresponding increase in the ΔD signal were observed until saturation was reached (Fig. 5**A**). The final Δf and ΔD shifts in the control case were around −131 Hz and 9 × 10^{-6}, respectively, whereas they were around −141 Hz and 9 × 10^{-6}, respectively, in the Mg^{2+} case. The adsorption kinetics and response magnitudes are consistent with intact vesicle adlayer formation [41–43]. Similar results were obtained in the Ca^{2+} case with one key caveat. While the responses in the Mg^{2+} case were larger than in the control case, the responses were smaller than the control case in the

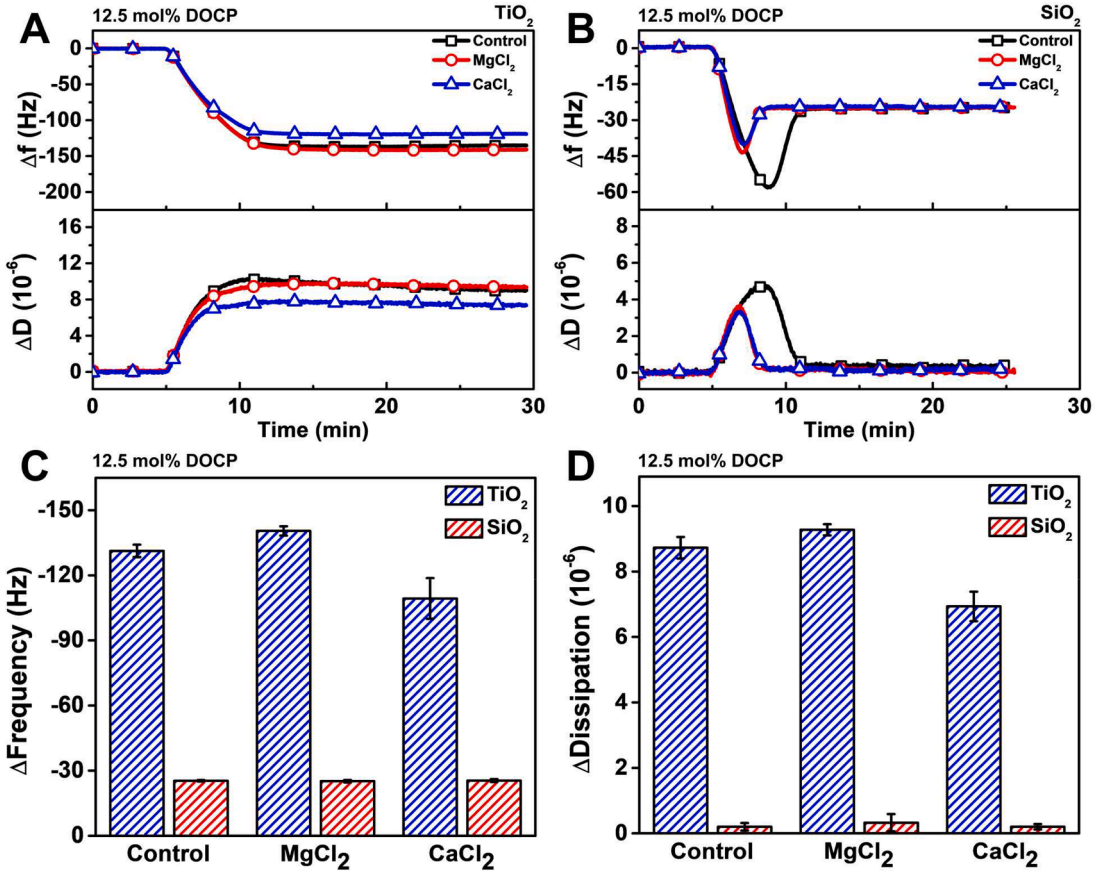

Fig. 5. QCM-D measurements tracking 12.5 mol% DOCP lipid vesicle adsorption onto TiO_2 and SiO_2 surfaces and divalent cation effects. The lipid composition of the vesicles was 12.5/87.5 mol% DOCP/DOPC and the panels are depicted as in Fig. 3.

Ca^{2+} case. The corresponding Δf and ΔD shifts were around −109 Hz and 7×10^{-6}, respectively, and indicate that Ca^{2+} caused more extensive deformation of adsorbed vesicles on TiO_2 due to stronger vesicle-surface interactions. Of note, while there are DOCP-TiO_2 bonding interactions in this case, the tether-like bond density is not sufficiently large to trigger vesicle rupture and divalent cations do not appear to enhance this effect appreciably.

On SiO_2, SLB formation with two-step kinetics was observed in all cases, with typical final Δf and ΔD values around −26 Hz and 0.5×10^{-6}, respectively (Fig. 5**B**). At the inflection point denoting the critical coverage, the Δf and ΔD shifts in the control case were around −58 Hz and 5×10^{-6}, respectively. Smaller critical coverage values occurred in the presence of Mg^{2+} ($\Delta f \sim -44$ Hz and $\Delta D \sim 4 \times 10^{-6}$) and Ca^{2+} ($\Delta f \sim -40$ Hz and $\Delta D \sim 3 \times 10^{-6}$) ions, indicating that both divalent cation types caused more extensive vesicle deformation on SiO_2 and also accelerated the SLB formation process. In summary, the 12.5 mol% DOCP lipid vesicles form intact vesicle adlayers on TiO_2 and SLBs on SiO_2, with divalent cations modulating the extent of vesicle-surface interactions and corresponding kinetic processes (Figs. 5**C,D**).

Together, the QCM-D data support that divalent cations impede 100 mol% DOCP lipid vesicle adsorption on both surfaces, whereas they enable SLB formation for 25 mol% DOCP lipid vesicles on both surfaces except in the case of Mg^{2+} on TiO_2 (Fig. 6). On the other hand, 12.5 mol % DOCP lipid vesicles adsorb and remain intact on TiO_2 while divalent cations have only slight effect in that case. Additionally, divalent cations accelerate SLB formation on SiO_2 for 12.5 mol% DOCP lipid vesicles.

3.4. Lipid attachment

We also measured the extent of lipid adlayer remaining on the oxide surfaces after ethanol washing, which removes weakly adsorbed lipid molecules except for those firmly attached by covalent or other strong noncovalent forces. The amount of remaining lipid was judged by QCM-D measurements whereby ethanol washing was performed after vesicle adsorption in buffer, followed by exchange back to buffer solution at the end. The resulting Δf shift values were compared relative to the original buffer baseline. In the case of DOCP SLBs on TiO_2 surfaces, the ethanol washing step removes the upper leaflet while the lower leaflet (monolayer) remains attached on the sensor surface, for example [14]. In cases where negligible vesicle adsorption occurred, the final Δf shifts were directly reported from the adsorption data.

Fig. 7 presents the final Δf shifts of adsorbed lipid layers on TiO_2 and SiO_2 surfaces. As a guiding reference, for a typical self-assembled monolayer, the final Δf shift ranges from around −10 to −15 Hz (roughly in the range of −13 Hz depending on chain properties) [39]. Based on this criterion, there was monolayer formation on TiO_2 with 100 mol% DOCP vesicles in the control case and the final Δf shift after ethanol washing was around −13 Hz (Fig. 7**A**). By contrast, in the Mg^{2+} and Ca^{2+} cases, there was negligible lipid attachment, which stems from the lack of vesicle adsorption in the corresponding buffer solutions in those cases. For 25/75 mol% and 12.5/87.5 mol% DOCP/DOPC lipid vesicles, the final Δf shifts fell within the monolayer range in all cases, indicating strong lipid-surface attachment. Although SLB formation did not occur in the control and Mg^{2+} cases for 25/75 mol% DOCP/DOPC lipid vesicles and in all cases for 12.5/87.5 mol% DOCP/DOPC vesicles, the final Δf shifts after ethanol rinsing were similar to cases where SLB formation occurred and are consistent with monolayer formation. This finding supports that strong lipid attachment is still possible on TiO_2 in spite of insufficiently strong vesicle-surface interactions that are necessary to trigger complete vesicle rupture.

Fig. 7**B** presents the corresponding results for lipid attachment on SiO_2 after ethanol washing. Interestingly, the final Δf shifts for the 25/75 mol% and 12.5/87.5 mol% DOCP/DOPC lipid vesicle cases indicated that the remaining attached lipids had values within the range of monolayers, supporting that the lipids are firmly attached to the SiO_2 surface. While DOCP lipids do not form covalent bonds with SiO_2 surfaces [3], the outward presentation of the phosphate group plays a key role in the strong attachment whereas typical, zwitterionic DOPC lipids are fully washed away from the SiO_2 interface upon ethanol rinsing. Specifically, the outward-facing phosphate group of DOCP lipids likely forms a strong hydrogen-bonding interaction with the SiO_2 surface (~14 kcal/mol per hydrogen bond) [44].

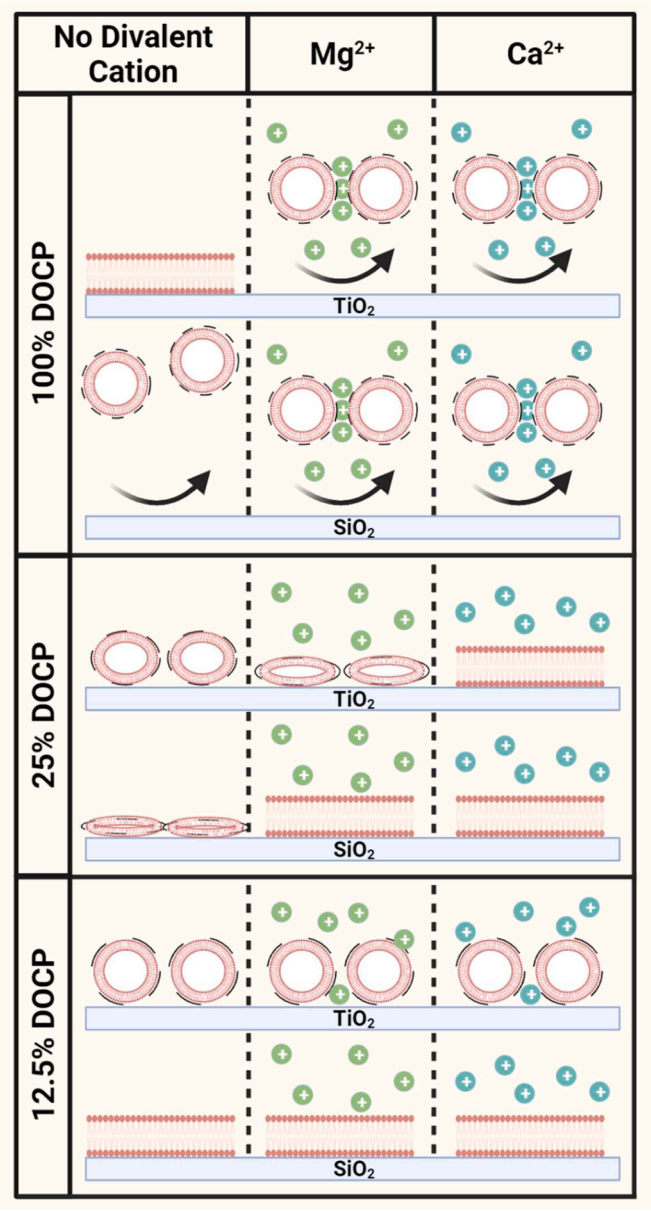

Fig. 6. Schematic summary. Self-assembly outcomes for DOCP lipid-containing vesicles on TiO_2 and SiO_2 surfaces in the absence and presence of divalent cations.

We were intrigued by strong DOCP lipid attachment on SiO_2 surfaces and further investigated that system, focusing on the 25/75 mol% DOCP/DOPC lipid vesicle case since the vesicle-surface interaction was sufficient to trigger vesicle rupture and SLB formation in both divalent cation cases. After SLB formation in the presence of Mg^{2+} or Ca^{2+}, an equivalent buffer containing 5 mM ethylenediaminetetraacetic acid (EDTA), which is known to chelate Mg^{2+} and Ca^{2+} ions, was injected to remove divalent cations, followed by another exchange step to equivalent buffer without EDTA and then the ethanol washing step, followed by final buffer exchange.

Fig. 8 presents QCM-D and fluorescence recovery after

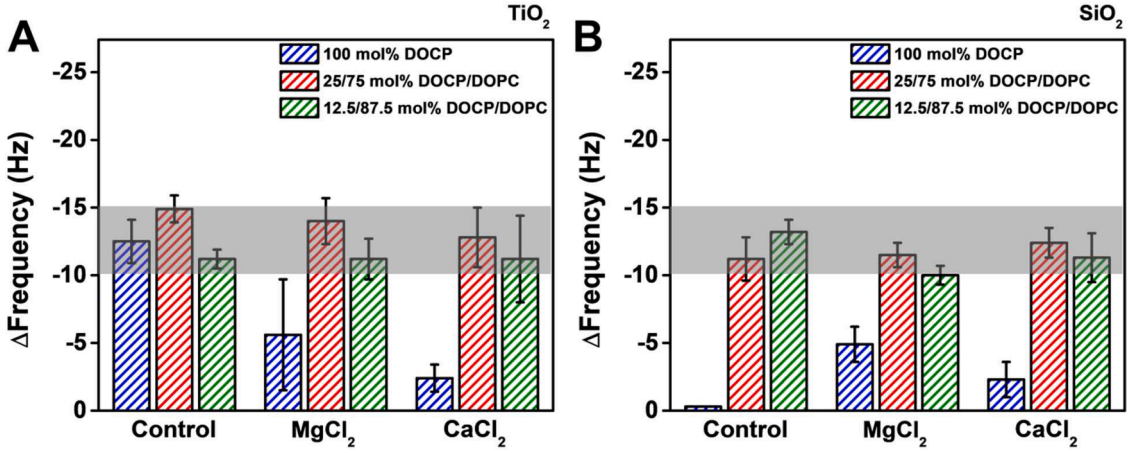

Fig. 7. QCM-D measurements of adsorbed lipid layers after ethanol washing. Frequency (Δf) shifts corresponding to attached lipid molecules on **(A)** TiO_2 and **(B)** SiO_2 after ethanol wash and subsequent buffer wash. The shifts are reported relative to baseline measurements in equivalent buffer prior to vesicle addition, and the Δf shifts correspond to the lipid layer that remains bound on the surface. The shaded region represents the typical range of Δf shifts for a lipid monolayer. The mean ± standard deviation are reported from three independent measurements.

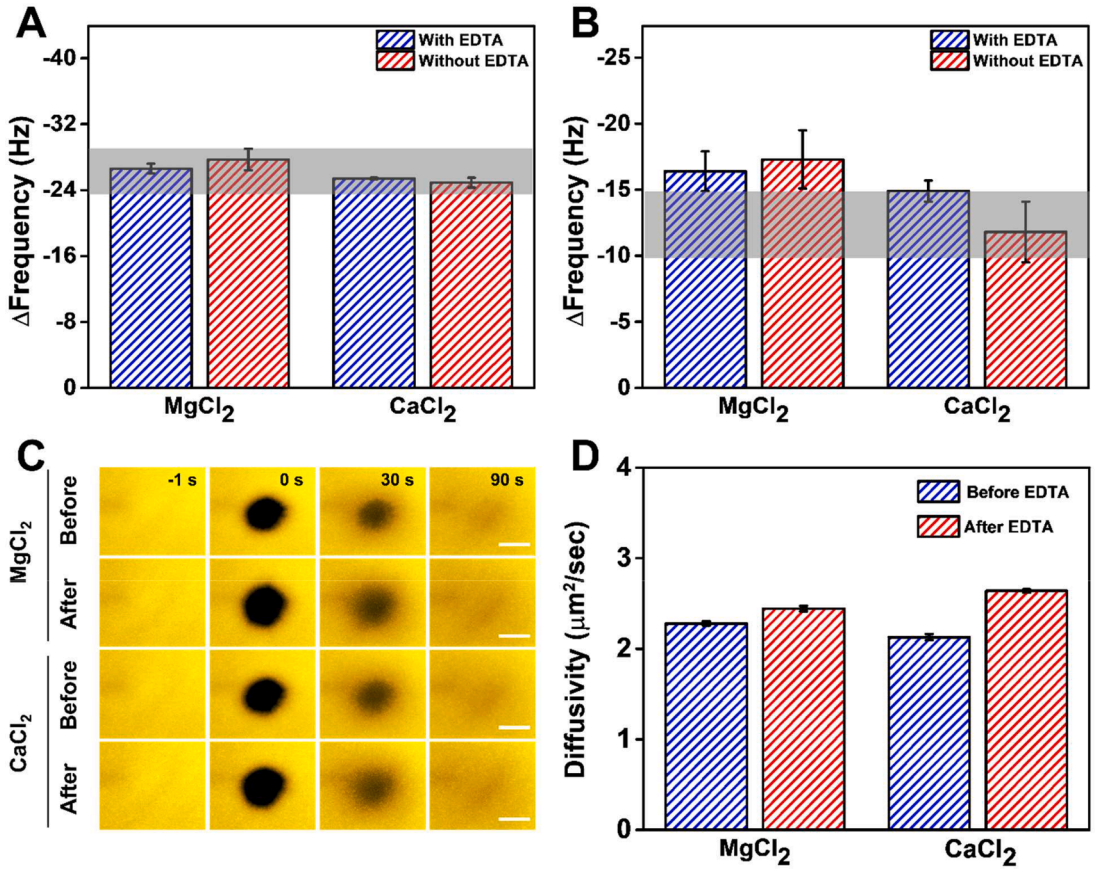

Fig. 8. Effect of divalent cation removal on adlayer properties of DOCP/DOPC supported lipid bilayers. Supported lipid bilayers (SLBs) were fabricated on SiO_2 surfaces by utilizing 25/75 mol% DOCP/DOPC lipid vesicles. In the QCM-D experiments, the baseline signal was established in buffer without divalent cations. The buffer was then switched to buffer with divalent cations (5 mM $MgCl_2$ or $CaCl_2$) and vesicles were added in equivalent buffer to form the SLB, followed by washing with the same buffer (without vesicles). Afterwards, for the "With EDTA" group (blue color), the following steps were performed: (i) injection of buffer containing 5 mM EDTA, (ii) injection of buffer without divalent cations, (iii) ethanol wash, and (iv) injection of buffer without divalent cations. The final frequency (Δf) shifts corresponding to **(A)** SLB formation [prior to step (i)] and **(B)** the remaining lipid adlayer after ethanol washing [after step (iv)]. For the "Without EDTA" group (red color), similar experiments were performed without step (i). The mean ± standard deviation are reported from three measurements. **(C)** FRAP images of fluorescently doped SLB before and after EDTA treatment (blue and red colors, respectively). After SLB fabrication, the FRAP experiment was first performed in the same buffer containing divalent cations and again performed after EDTA treatment and exchange to equivalent buffer solution without divalent cations. The scale bars are 20 μm. **(D)** Corresponding diffusion coefficients of lateral lipid mobility for the SLBs presented in panel (C). The mean ± standard deviation are reported from five measurements.

photobleaching (FRAP) characterization data of the fabricated SLBs and resulting lipid adlayers (due to ethanol washing) without or with EDTA treatment. The QCM-D data indicated that EDTA treatment and resulting divalent cation removal did not appreciably affect the measured Δf shifts corresponding to the SLB properties (Fig. 8**A**). Similarly, the removal of divalent cations did not have a strong effect on the remaining lipid adlayer properties after ethanol washing (Fig. 8**B**). In the Ca^{2+} case, the Δf shifts tended to decrease from approximately −14 Hz to −11 Hz but no effect was observed in the Mg^{2+} case. Interestingly, the final Δf shifts in the Mg^{2+}case in this experimental series were slightly higher than the typical monolayer range and may relate to Mg^{2+} enhancing DOCP-SiO_2 interactions by acting as a bridging ligand.

To further characterize the SLB formed on SiO_2 formed from 25/75 mol% DOCP/DOPC lipid vesicles, FRAP experiments were also performed. Fig. 8**C** presents time-lapse snapshots of fluorescently labeled SLBs formed from vesicles in the Mg^{2+}- or Ca^{2+}-containing buffers, either in that buffer directly after SLB formation and buffer washing ("Before EDTA") or after subsequent EDTA treatment and exchange to equivalent buffer without divalent cations ("After EDTA"). The bleached spots recovered fluorescence intensity over a 2-min period, which is evidence of lateral lipid mobility. The diffusion coefficients in each case were also quantified (Fig. 8**D**). The SLB mobility values on SiO_2 in the presence of Mg^{2+} and Ca^{2+} were 2.28 ± 0.02 $\mu m^2/sec$ and 2.13 ± 0.03 $\mu m^2/sec$, respectively, which are consistent with literature values for fluid-phase SLBs [45,46]. After EDTA treatment, the respective mobility values were 2.44 ± 0.03 $\mu m^2/sec$ in the Mg^{2+} case and 2.64 ± 0.02 $\mu m^2/sec$ in the Ca^{2+} case, which equated to mobility increases of ~7 % and ~24 %. Thus, a modest increase in the diffusion coefficients occurred upon removal of divalent cations while the effect was modest and supports that divalent cations enhance DOCP-SiO_2 interactions but do not impede SLB fluidity.

Regarding the ability to control SLB fabrication on TiO_2 and SiO_2 surfaces by using divalent cations, we would like to further emphasize that nanomechanical stability is another important design factor in addition to forming the SLB coating itself [47,48]. In particular, it has been discussed how chemical and topographical modulation of the underlying substrate can influence the thermal and osmotic stability of hybrid SLBs composed of zwitterionic phospholipids due to variations in how the lower leaflet [*i.e.*, the self-assembled monolayer (SAM)] is organized [49]. Extending such studies to phosphate-functionalized SAM molecules, including DOCP and single-chain analogues, on flat surfaces and more topographically complex ones is warranted to further unravel how hybrid SLB stability is influenced in general and by the presence of divalent cations in particular.

Conclusion

Recent progress in the nanobioscience field has demonstrated that CP lipid coatings have attractive merits such as facilitating versatile chemical functionalization options and durable attachment to certain materials. However, a key limitation of CP lipids is that they only form SLB coatings on a limited range of materials whereas they do not attach to other commonly used materials like SiO_2. Controlling the molecular self-assembly of CP lipids on inorganic material interfaces has been the focus of ongoing research and an interplay of covalent and noncovalent forces is known to drive the vesicle adsorption process and dictates the self-assembly outcome. In the present study, we have identified that a third factor – ionic bridging interactions between vesicles and surfaces that are mediated by divalent cations – can play a crucial role in transforming the self-assembly pathway. For example, divalent cations prevent vesicle adsorption in cases where SLBs would form otherwise, and they can also enable SLB formation on both TiO_2 and SiO_2 surfaces under the same conditions whereas CP lipids typically have repulsive interactions with SiO_2. While the fabricated SLBs demonstrated high lateral fluidity values, the ability to easily remove the divalent cations post-fabrication can further enhance fluidity and enables tunable control over the lipid membrane platform design and environmental conditions.

CRediT authorship contribution statement

Tun Naw Sut: Conceptualization, Methodology, Investigation, Writing – original draft, Writing – review & editing. **Soohyun Park:** Methodology, Investigation, Writing – review & editing. **Joshua A. Jackman:** Conceptualization, Methodology, Investigation, Writing – original draft, Writing – review & editing, Supervision. **Nam-Joon Cho:** Conceptualization, Methodology, Investigation, Writing – original draft, Writing – review & editing, Supervision.

Declaration of Competing Interest

The authors declare that they have no known competing financial interests or personal relationships that could have appeared to influence the work reported in this paper.

Data availability

The data that has been used is confidential.

Acknowledgments

This work was supported by the Ministry of Education (MOE) in Singapore under grants RG111/20 and RG34/22 and by National Research Foundation of Korea (NRF) grants funded by the Korean government (MSIT) (Nos. 2020R1C1C1004385, 2021R1A4A1032782, 2022K1A3A1A39085112). In addition, this work was supported under the framework of international cooperation program managed by the National Research Foundation (NRF) of Korea (2022K2A9A2A12000287, FY2022) and by the Basic Science Research Program through the National Research Foundation of Korea (NRF) funded by the Ministry of Education (No. RS-2023-00246169). This work was also partially supported by the SKKU Global Research Platform Research Fund, Sungkyunkwan University, 2023.

References

[1] E.K. Perttu, A.G. Kohli, F.C. Szoka Jr, Inverse-phosphocholine lipids: a remix of a common phospholipid, J. Am. Chem. Soc. 10 (2012) 4485–4488.
[2] F. Wang, X. Zhang, Y. Liu, Z.Y.W. Lin, B. Liu, J. Liu, Profiling metal oxides with lipids: magnetic liposomal nanoparticles displaying DNA and proteins, Angew. Chem. Int. Ed. 39 (2016) 12063–12067.
[3] F. Wang, J. Liu, A stable lipid/TiO_2 interface with headgroup-inversed phosphocholine and a comparison with SiO_2, J. Am. Chem. Soc. 36 (2015) 11736–11742.
[4] S. Li, F. Wang, X. Li, J. Chen, X. Zhang, Y. Wang, J. Liu, Dipole orientation matters: longer-circulating choline phosphate than phosphocholine liposomes for enhanced tumor targeting, ACS Appl. Mater. Interfaces 21 (2017) 17736–17744.
[5] J. Motion, J. Nguyen, F.C. Szoka, Phosphatase-triggered fusogenic liposomes for cytoplasmic delivery of cell-impermeable compounds, Angew. Chem. 36 (2012) 9181–9185.
[6] L. Wang, N. Malmstadt, Interactions between charged nanoparticles and giant vesicles fabricated from inverted-headgroup lipids, J. Phys. D Appl. Phys. 41 (2017), 415402.
[7] A.G. Kohli, P.H. Kierstead, V.J. Venditto, C.L. Walsh, F.C. Szoka, Designer lipids for drug delivery: from heads to tails, J. Controlled Release (2014) 274–287.
[8] Y. Liu, F. Wang, J. Liu, Headgroup-inversed liposomes: biointerfaces, supported bilayers and applications, Langmuir 32 (2018) 9337–9348.
[9] X. Li, Y. Zhao, W. Jiang, S. Li, M. Zhan, H. Liu, C. Zhang, H. Liang, H. Liu, L. Lu, Ultralong circulating choline phosphate liposomal nanomedicines for cascaded chemo-radiotherapy, Biomater. Sci. 4 (2019) 1335–1344.
[10] S. Meker, O. Halevi, H. Chin, T.N. Sut, J.A. Jackman, E.-L. Tan, M.G. Potroz, N.-J. Cho, Inkjet-printed phospholipid bilayers on titanium oxide surfaces: towards functional membrane biointerfaces, Membranes 4 (2022) 361.
[11] A. Mashaghi, S. Mashaghi, I. Reviakine, R.M. Heeren, V. Sandoghdar, M. Bonn, Label-free characterization of biomembranes: from structure to dynamics, Chem. Soc. Rev. 3 (2014) 887–900.

[12] T.N. Sut, S.W. Tan, W.-Y. Jeon, B.K. Yoon, N.-J. Cho, J.A. Jackman, Streamlined fabrication of hybrid lipid bilayer membranes on titanium oxide surfaces: a comparison of one-and two-tail SAM molecules, Nanomaterials 7 (2022) 1153.
[13] S.P. Pujari, L. Scheres, A. Marcelis, H. Zuilhof, Covalent surface modification of oxide surfaces, Angew. Chem. Int. Ed. 25 (2014) 6322–6356.
[14] T.N. Sut, A.R. Ferhan, S. Park, D.J. Koo, B.K. Yoon, J.A. Jackman, N.-J. Cho, Modulating noncovalent and covalent forces to control inverse phosphocholine lipid self-assembly on inorganic surfaces: nanoarchitectonic design principles, Appl. Mater. Today (2022), 101618.
[15] T.N. Sut, S. Meker, D. Jun Koo, J.A. Jackman, N.-J. Cho, Interfacial approach to fabricate covalently and noncovalently attached inverse-phosphocholine supported lipid bilayers on TiO_2 and SiO_2 surfaces, J. Ind. Eng. Chem. (2023), https://doi.org/10.1016/j.jiec.2023.07.053.
[16] R. Richter, A. Mukhopadhyay, A. Brisson, Pathways of lipid vesicle deposition on solid surfaces: a combined QCM-D and AFM study, Biophys. J. 5 (2003) 3035–3047.
[17] S. Garcia-Manyes, G. Oncins, F. Sanz, Effect of ion-binding and chemical phospholipid structure on the nanomechanics of lipid bilayers studied by force spectroscopy, Biophys. J. 3 (2005) 1812–1826.
[18] F.F. Rossetti, M. Bally, R. Michel, M. Textor, I. Reviakine, Interactions between titanium dioxide and phosphatidyl serine-containing liposomes: formation and patterning of supported phospholipid bilayers on the surface of a medically relevant material, Langmuir 14 (2005) 6443–6450.
[19] J. Ekeroth, P. Konradsson, F. Höök, Bivalent-ion-mediated vesicle adsorption and controlled supported phospholipid bilayer formation on molecular phosphate and sulfate layers on gold, Langmuir 21 (2002) 7923–7929.
[20] M. Dacic, J.A. Jackman, S. Yorulmaz, V.P. Zhdanov, B. Kasemo, N.-J. Cho, Influence of divalent cations on deformation and rupture of adsorbed lipid vesicles, Langmuir 25 (2016) 6486–6495.
[21] J. Wilschut, N. Duzgunes, R. Fraley, D. Papahadjopoulos, Studies on the mechanism of membrane fusion: kinetics of calcium ion induced fusion of phosphatidylserine vesicles followed by a new assay for mixing of aqueous vesicle contents, Biochemistry 26 (1980) 6011–6021.
[22] A. Portis, C. Newton, W. Pangborn, D. Papahadjopoulos, Studies on the mechanism of membrane fusion: evidence for an intermembrane Ca^{2+}-phospholipid complex, synergism with Mg^{2+}, and inhibition by spectrin, Biochemistry 5 (1979) 780–790.
[23] E.M. Kerek, E.J. Prenner, Inorganic cadmium affects the fluidity and size of phospholipid based liposomes, Biochim. Biophys. Acta Biomemb. 12 (2016) 3169–3181.
[24] Y. Liu, J. Liu, Zn^{2+} induced irreversible aggregation, stacking, and leakage of choline phosphate liposomes, Langmuir 50 (2017) 14472–14479.
[25] Y. Liu, J. Liu, Cu^{2+}-directed liposome membrane fusion, positive-stain electron microscopy, and oxidation, Langmuir 25 (2018) 7545–7553.
[26] R.C. MacDonald, R.I. MacDonald, B.P.M. Menco, K. Takeshita, N.K. Subbarao, L.-r. Hu, Small-volume extrusion apparatus for preparation of large, unilamellar vesicles, Biochim. Biophys. Acta Biomemb. 2 (1991) 297–303.
[27] B.J. Berne, R. Pecora, Dynamic light scattering: with applications to chemistry, Biol. Phys., Courier Corp. (2000).
[28] J.A. Jackman, S.R. Tabaei, Z. Zhao, S. Yorulmaz, N.-J. Cho, Self-assembly formation of lipid bilayer coatings on bare aluminum oxide: overcoming the force of interfacial water, ACS Appl. Mater. Interfaces 1 (2015) 959–968.
[29] P. Jönsson, M.P. Jonsson, J.O. Tegenfeldt, F. Höök, A method improving the accuracy of fluorescence recovery after photobleaching analysis, Biophys. J. 11 (2008) 5334–5348.
[30] E. Kerek, M. Hassanin, E.J. Prenner, Inorganic mercury and cadmium induce rigidity in eukaryotic lipid extracts while mercury also ruptures red blood cells, Biochim. Biophys. Acta Biomemb. 3 (2018) 710–717.
[31] R. Koynova, M. Caffrey, Phases and phase transitions of the phosphatidylcholines, Biochim. Biophys. Acta (BBA)-Rev. Biomembr. 1 (1998) 91–145.
[32] P. Van Dijck, B. De Kruijff, A. Verkleij, L. Van Deenen, J. De Gier, Comparative studies on the effects of pH and Ca^{2+} on bilayers of various negatively charged phospholipids and their mixtures with phosphatidylcholine, Biochim. Biophys. Acta 1 (1978) 84–96.
[33] J. Umbsaar, E. Kerek, E.J. Prenner, Cobalt and Nickel Affect the Fluidity of Negatively-Charged Biomimetic Membranes, Chem. Phys. Lipids. (2018) 28–37.
[34] K. Sule, M. Anikovskiy, E.J. Prenner, Lipid structure determines the differential impact of single metal additions and binary mixtures of manganese, calcium and magnesium on membrane fluidity and liposome size, Int. J. Mol. Sci. 2 (2023) 1066.
[35] G. Pabst, A. Hodzic, J. Štrancar, S. Danner, M. Rappolt, P. Laggner, Rigidification of neutral lipid bilayers in the presence of salts, Biophys. J. 8 (2007) 2688–2696.
[36] K. Balantič, V.U. Weiss, G. Allmaier, P. Kramar, Calcium ion effect on phospholipid bilayers as cell membrane analogues, Bioelectrochemistry (2022), 107988.
[37] N.-J. Cho, C.W. Frank, B. Kasemo, F. Höök, Quartz crystal microbalance with dissipation monitoring of supported lipid bilayers on various substrates, Nat. Protoc. 6 (2010) 1096–1106.
[38] B. Seantier, B. Kasemo, Influence of mono-and divalent ions on the formation of supported phospholipid bilayers via vesicle adsorption, Langmuir 10 (2009) 5767–5772.
[39] C. Keller, B. Kasemo, Surface specific kinetics of lipid vesicle adsorption measured with a quartz crystal microbalance, Biophys. J. 3 (1998) 1397–1402.
[40] E. Reimhult, F. Höök, B. Kasemo, Intact vesicle adsorption and supported biomembrane formation from vesicles in solution: influence of surface chemistry, vesicle size, temperature, and osmotic pressure, Langmuir 5 (2003) 1681–1691.
[41] J.A. Jackman, G.H. Zan, Z. Zhao, N.-J. Cho, Contribution of the hydration force to vesicle adhesion on titanium oxide, Langmuir 19 (2014) 5368–5372.
[42] N.-J. Cho, J.A. Jackman, M. Liu, C.W. Frank, pH-driven assembly of various supported lipid platforms: a comparative study on silicon oxide and titanium oxide, Langmuir 7 (2011) 3739–3748.
[43] N.-J. Cho, C.W. Frank, Fabrication of a planar zwitterionic lipid bilayer on titanium oxide, Langmuir 20 (2010) 15706–15710.
[44] V.V. Murashov, J. Leszczynski, Adsorption of the phosphate groups on silica hydroxyls: an ab initio study, J. Phys. Chem. A 9 (1999) 1228–1238.
[45] T. Köchy, T.M. Bayerl, Lateral diffusion coefficients of phospholipids in spherical bilayers on a solid support measured by resonance 2 relaxation, Phys. Rev. E 3 (1993) 2109.
[46] S.R. Tabaei, J.-H. Choi, G. Haw Zan, V.P. Zhdanov, N.-J. Cho, Solvent-assisted lipid bilayer formation on silicon dioxide and gold, Langmuir 34 (2014) 10363–10373.
[47] A.L. Plant, Supported hybrid bilayer membranes as rugged cell membrane mimics, Langmuir 15 (1999) 5128–5135.
[48] L. Bar, M.E. Villanueva, S. Neupane, G. Cordoyiannis, P. Losada-Pérez, QCM-D study of the formation of solid-supported artificial lipid membranes: state-of-the-art, recent advances, and perspectives, Phys. Status Solidi (A) (2023), 2200625.
[49] L. Bar, M.E. Villanueva, C. Martín, A.V. Ramirez, J. Goole, F.U. Renner, P. Losada-Pérez, Stability of supported hybrid lipid bilayers on chemically and topographically-modified surfaces, Colloids Surf. A (2023), 131125.